scientific data

Check for updates

OPEN

DATA DESCRIPTOR

Single-Cell Transcriptomic Dataset of RPGR-associated Retinitis Pigmentosa Patient-Derived Retinal Organoids

Ting Li[1,2,3,4,7], Yuting Ma[5,6,7], Yun Cheng[2,3,4], Yingke Zhao[2,3,4], Zhixu Qiu[6], Hongli Liu[2,3,4], Daowei Zhang[2,3,4], Jiawen Wu[2,3,4], Junfeng Li[2,3,4], Shenghai Zhang[2,3,4] ✉ & Jihong Wu[1,2,3,4] ✉

X-linked retinitis pigmentosa (XLRP) is a severe hereditary retinal disorder marked by progressive vision loss due to photoreceptor dysfunction. The retinitis pigmentosa GTPase regulator (RPGR) gene, responsible for most XLRP cases, encodes a protein crucial for the transport of visual signal proteins between the photoreceptor inner and outer segments. However, the mechanism of RPGR mutation causing photoreceptor disorder is not clear and effective treatments remain elusive. This study utilized retinal organoids (ROs) derived from normal and RPGR-mutant human induced pluripotent stem cells (hiPSC) at four developmental stages (40, 90, 150, and 200 days). Single-cell RNA sequencing (scRNA-seq) was conducted on 71,096 cells, including 33,839 cells from the control group and 37,257 cells from the RPGR group. Key retinal cell types were identified and the obtained scRNAseq dataset was validated reliable and high -quality. This study has provided data resources and references for exploring the mechanism of RPGR-related retinal degeneration and support the development of targeted therapies.

Background and summary

X-linked retinitis pigmentosa (XLRP) is a hereditary retinal degenerative disorder characterized by the progressive loss of photoreceptor cell function and is considered to be the most severe form of retinitis pigmentosa (RP). Clinically, it presents with progressive visual field loss, decreased visual acuity, night blindness, distinctive fundus pigmentation, and abnormal electroretinograms, with an onset during the first decade of life, making it a significant cause of blindness in adolescents[1,2]. Among the genes associated with XLRP, the retinitis pigmentosa GTPase regulator (RPGR) gene is the first to be identified and the most significant, accounting for 70%-80% of cases[3,4]. In male patients, retinal degeneration is particularly severe and progresses rapidly, while RPGR female carriers exhibit variable phenotypes, from the most common asymptomatic presentation to uncommon early-onset severe disease[5]. The RPGR-encoded protein is typically found in the photoreceptor connecting cilium and involved in the transport of visual signal proteins between the photoreceptor inner and outer segments[6,7]. Knockout of RPGR in mice causes a mislocalization and downregulation of rhodopsin, notable abnormality of newly formed disk membranes, and finally a decrease in the thickness of the ONL (photoreceptor nuclei) at 8 months of age[8,9]. Extensive efforts have been made to elucidate the molecular mechanisms caused by RPGR mutations using animal models. However, the mechanisms by which RPGR mutations lead to RP are not yet fully understood, due to the challenges in obtaining and culturing human retinal tissues and the substantial genetic differences existing in the RPGR sequences across different species[10,11]. Despite advances in gene therapy, effective treatments for this type of retinal degenerative disease are still lacking. For developing therapeutic interventions, we still need to understand the molecular underpinnings of the disease.

[1]Qingdao Institute, College of Medicine, Fudan University, Qingdao, 266500, China. [2]Department of Ophthalmology, Eye and ENT Hospital, College of Medicine, Fudan University, Shanghai, 200000, China. [3]Shanghai Key Laboratory of Visual Impairment and Restoration, Science and Technology Commission of Shanghai Municipality, Shanghai, 200000, China. [4]Key Laboratory of Myopia (Fudan University), Chinese Academy of Medical Sciences, National Health Commission, Shanghai, 200000, China. [5]College of Life Sciences, University of Chinese Academy of Sciences, Beijing, 100049, China. [6]BGI Genomics, Shenzhen, 518083, China. [7]These authors contributed equally: Ting Li, Yuting Ma. ✉e-mail: zsheent@163.com; jihongwu@fudan.edu.cn

With breakthroughs in technology of human induced pluripotent stem cell (hiPSC) reprogrammed from somatic cells, hiPSC-derived organoids offer new and robust research tools to construct disease models *in vitro*, to study underlying cellular and molecular mechanisms, drug screening, and exploratory replacement therapies[12]. Retinal organoids (ROs) are generated from hiPSC self-assembling into retinal progenitor spheres, from which differentiate into various retinal cell types and organizing into a structure that closely resembles the *in vivo* retina. ROs act as *in vitro* models that can be rapidly constructed to closely replicate real human conditions and retain the highly similar genetic backgrounds and histological characteristics of the source tissue[13].

The advent of single-cell RNA sequencing (scRNA-seq) technology allows for the sequencing and analysis of transcriptomes from individual retinal cells, enabling precise cell classification and exploration of their physiological functions and developmental characteristics. The rate of transcriptomic changes during organoid development mirrors that of *in vivo* human retinal development, and the transcriptomes of cell types in organoids converge with those of the adult peripheral retina[14–16]. A comparative genetic disease map, generated by comparing the expression of disease-related genes in organoids and target organs, reveals that retinal diseases exhibit cell type specificity, which is preserved in organoids[17].

In this study, we successfully constructed retinal organoids from normal and RPGR-mutant iPSCs. We obtained single-cell transcriptomes from 71,096 cells isolated from organoids at four different developmental time points (40 days, 90 days, 150 days, 200 days). Through single-cell transcriptome analysis, we identified various cell types, including early and late retinal progenitor cells (RPC), retinal ganglion cells (RGC), bipolar cells (BC), horizontal cells (HC), amacrine cells (AC), photoreceptor precursors, cone photoreceptors, rod photoreceptors and müller cells. Our study reveals the transcriptomic characteristics of retinal organoid development at different stages in the context of RPGR mutations and provides a comparative map of cell type-specific transcriptomes between healthy retinal organoids and those affected by retinitis pigmentosa. This foundational work supports further research into disease mechanisms and targeted therapies.

Materials and Methods

Retinal organoids culture and samplings. The study was approved by the Ethics Review Committee of the Eye, Ear, Nose and Throat Hospital, Fudan University (Approval ID: 2019025) and the patient involved in this project has signed an informed consent form and consented to data sharing. After obtaining informed consent, venous blood was collected from the patient, who was diagnosed with typical clinical manifestations of RP, while the gene mutation was detected using whole-exome sequencing, identified as the deletion of exons 14-15 in the RPGR gene. hiPSC was generated from blood as previously described[18]. Peripheral blood mononuclear cells were isolated, CD34+ cells were magnetically separated and reprogrammed to hiPSC by electroporating with the episomal plasmids pCE-hOCT3/4, pCE-hSK, pCE-hUL, pCE-mp53DD and pCXB-EBNA1 (Addgene, #ID41813, #ID41814, #ID41855, #ID 41856, #ID41857)[19]. The control hiPSC was obtained from the Shanghai Institute of Biochemistry and Cell Biology Stem Cell Bank (DYR0100). Based on the documentation, this cell line was generated by reprogramming foreskin fibroblasts from a newborn using the transcription factors OCT4, SOX2, KLF4, and MYC. Culture of 3D human retinal organoids from hiPSCs was performed according to a previously described protocol[20]. In brief, hiPSCs were grown to 80% confluency in mTeSR™ Plus medium and gently dissociated to form embryoid bodies (EBs), at which time defined as day 0 (D0). EBs were cultured in suspension in neural induction medium (NIM) before plating on dishes covered by growth factor reduced Matrigel on day 7 (D7) and half medium changes of NIM until day15 to gradually dilute the BMP4 (1.5 nM, added to fresh NIM on day 6). Retinal differentiation medium (RDM) were henceforth given for the development of optic vesicles (OVs). 3D OVs were isolated using a pipette tip on day 30 (D30) and transitioned to suspension culture for retinal maturation and long-term culture of organoids, with feeding of 3D-RDM. Details of differentiation medium are given in Table S1. Developing ROs (2-3 samples) were collected for scRNA-seq on D40, D90, D150 and D200.

Immunofluorescence and Imaging. ROs were fixed in 4% paraformaldehyde for about 12 hours and then immersed in 30% sucrose overnight. After orientation in optimal cutting temperature compound (OCT) under a microscope, samples were frozen and sectioned into 10-μm slices. For immunocytochemistry, slides were blocked in Immunol Staining Blocking Buffer (Beyotime, #P0102) for 1 hour before incubation with primary antibodies for 2 hours (L/M-opsin, Sigma-Aldrich, #AB5405; NRL, Santa Cruz, #sc374277). Secondary antibodies (anti-mouse and anti-rabbit) were applied with careful avoidance of light for 1 hour (Thermo Fisher), and nuclei were stained with Hoechst (1:1000 in PBS) for visualization. The fluorescence images were acquired using a Zeiss Imager Z2 and a Stellaris laser scanning confocal microscope. The measurement of ONL thickness was performed using Fiji in the DAPI channel.

Single cell isolation for scRNA-seq. ROs collected were immediately isolated into single-cell suspension. Briefly, ROs were incubated in papain solution (Worthington, #LS003126) for about 15–20 minutes at 37°C, with gentle pipetting every 5 minutes, until cell clumps were dissociated into single cell suspension. The extent of dissociation was determined by bright-field microscopy. Enzymatic digestion was terminated through the addition of 4 times volume of 5% bovine serum albumin (BSA; Sigma, #A9056) in RPMI 1640 medium (Gibco, #11875093). The cells were pelleted by centrifuging 5 minutes at 1000 rpm and 4 °C and resuspended in RPMI for a 10XGenomics scRNA-experiment.

10X Genomics Library construction. The scRNA-Seq libraries were generated using the 10X Genomics Chromium Controller Instrument and Chromium Single Cell 3' V3.1 Reagent Kits (10X Genomics, Pleasanton, CA). Briefly, cells were concentrated to approximately 1000 cells/uL and loaded into each channel to generate

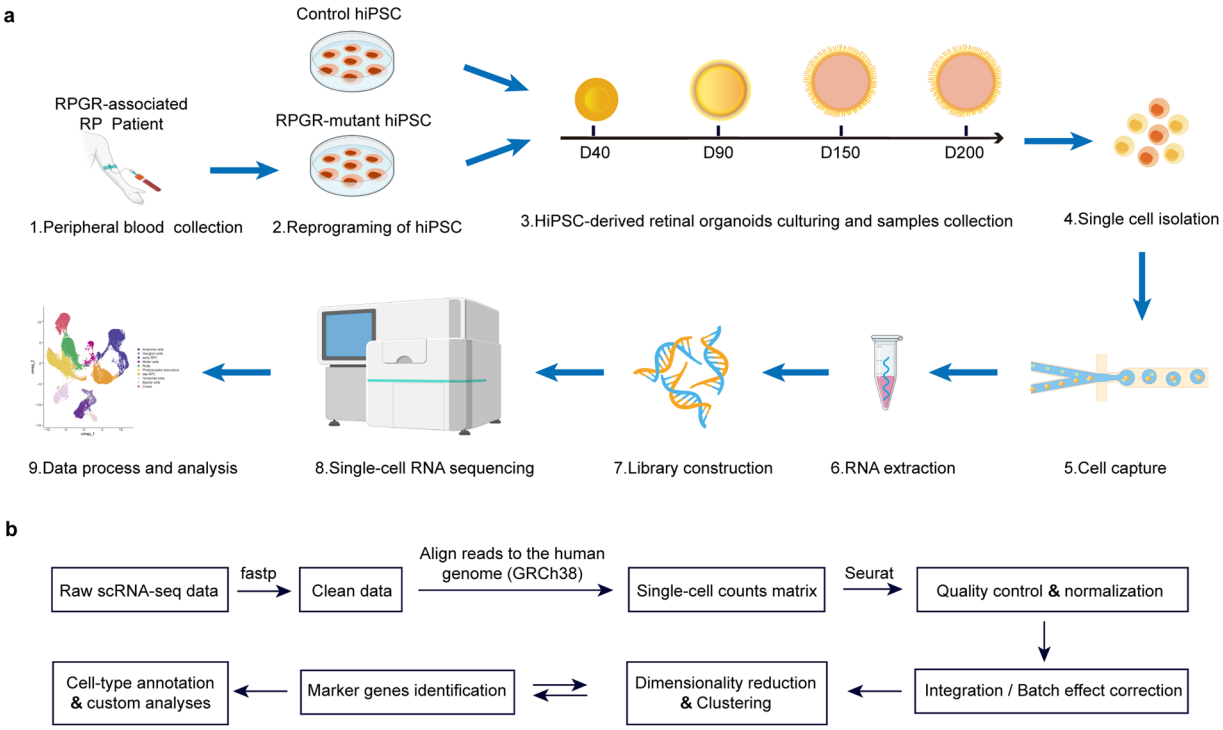

Fig. 1 The study workflow of scRNA-seq and data analysis. (**a**) Sample preparation and single-cell RNA sequencing. (1) Venous blood samples from a patient with RPGR retinitis pigmentosa were collected. (2) CD34+ cells were isolated from the fresh peripheral blood and electroporated with reprogramming vector to generate hiPSC. Control hiPSC were obtained from Shanghai Institute of Biochemistry and Cell Biology Stem Cell Bank (DYR0100). (3) HiPSC were progressively differentiated into isolated 3D retinal organoids in suspension culture using an established protocol. Developing ROs (2-3 samples) were collected on D40, D90, D150 and D200. (4) Prepare single-cell suspension of ROs for scRNA-seq by incubating in papain solution. (5) Single cells were captured, isolated and loaded into each channel to generate single-cell Gel Bead-In-Emulsions (GEMs). (6) RNA was extracted and barcoded-cDNA was amplified. (7) The scRNA-Seq libraries were generated using the 10X Genomics Chromium Controller Instrument. (8) scRNA-seq was performed using the illumina sequencer on a 150 bp paired-end run. (9) Processing raw scRNA-seq data and biological analysis. (**b**) Flow chart of scRNA- Seq data analysis.

single-cell Gel Bead-In-Emulsions (GEMs). After the reverse transcription (RT) step, GEMs were broken and barcoded-cDNA was purified and amplified. The amplified barcoded cDNA was fragmented, A-tailed, ligated with adaptors and index PCR amplified. The final libraries were quantified using the Qubit High Sensitivity DNA assay (Thermo Fisher Scientific) and the size distribution of the libraries were determined using a High Sensitivity DNA chip on a Bioanalyzer 2200 (Agilent). All libraries were sequenced by Illumina NovaSeq6000 (Illumina, San Diego, CA) on a 150 bp paired-end run.

Initial processing of the original scRNA-seq data. ScRNA-seq data analysis was performed by NovelBio Co., Ltd. with NovelBrain Cloud Analysis Platform (www.novelbrain.com). Before read mapping, we applied fastp (v0.21.0) with default parameter filtering the adaptor sequence and removed the low-quality reads to achieve the clean data. Detailly, reads with >5% ambiguous bases (noted as N) and low-quality reads containing more than 40 percent of bases with qualities of <15. Then the single-cell counts matrix was obtained by aligning reads to the human genome (GRCh38, Ensemble version 104) using CellRanger (v7.1.0) with include-introns mode. This mode helps to capture and align reads that map to both exonic (coding) and intronic (non-coding) regions of genes.

Quality control and normalization. Quality control (QC) is essential to ensure the reliability of downstream analyses. Cells were filtered based on gene counts, retaining those with counts between 500 and 8,000, and excluding cells with mitochondrial RNA (mtRNA) content exceeding 10%, to eliminate those likely to be stressed or damaged. To address technical biases and enhance biological interpretations, normalization and scaling were conducted following QC using Seurat (v4.1.1) in R (v4.1.2), ensuring that the downstream analysis is driven by relevant biological phenomena and not technical noise. The "NormalizeData" function normalized gene expression levels across all cells, and the "ScaleData" function scaled the normalized data to facilitate the identification of biologically relevant genes.

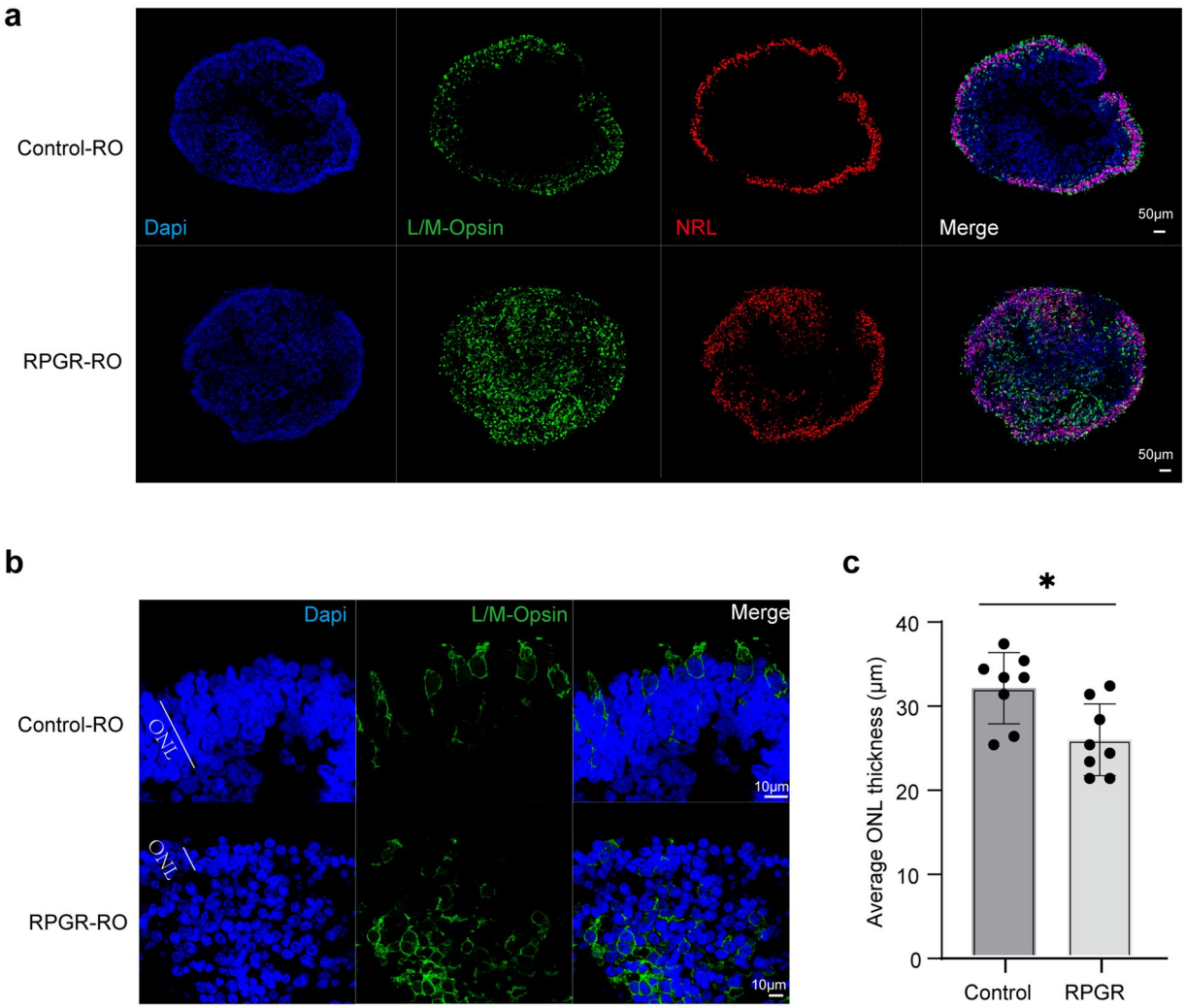

Fig. 2 Mature RPGR-mutant retinal organoids (D200) show diseased photoreceptors. (**a**) L/M opsin and NRL abnormalities in RPGR-mutant ROs. (**b**) L/M opsin mislocalization in RPGR-mutant ROs. (**c**) Mean ONL thickness per organoid (n = 8 independent organoids; $P < 0.05$; mean ± SD).

Sample names	Number of reads	Valid barcodes	Sequencing saturation	Q30 bases in barcode	Q30 bases in RNA read	Q30 bases in UMI	Confident mapping to genome	Confident mapping to transcriptome
Control-D40	334,054,977	98.40	59.70%	97.00%	93.30%	96.50%	94.40%	75.30%
Control-D90	343,845,921	97.90%	57.60%	96.90%	92.60%	96.40%	93.20%	66.00%
Control-D150	362,178,116	91.50%	55.80%	95.60%	91.50%	94.80%	89.60%	62.30%
Control-D200	341,410,195	98.30%	59.30%	96.30%	92.10%	95.80%	94.00%	64.80%
RPGR-D40	421,113,957	98.10%	56.00%	96.90%	92.80%	96.80%	93.60%	70.20%
RPGR-D90	316,166,350	97.60%	60.80%	96.80%	92.30%	96.40%	94.50%	63.60%
RPGR-D150	337,632,103	97.80%	58.20%	95.50%	91.90%	95.20%	94.60%	67.10%
RPGR-D200	322,841,201	97.9%	51.8%	96.4%	92.3%	95.9%	93.5%	63.6%

Table 1. Detailed quality control of raw scRNA-seq data.

Doublet Removal. Doublets were removed using the "DoubletFinder" package (v2.0.3). The process involved performing principal component analysis (PCA) on the normalized data to achieve dimensionality reduction, generating simulated doublet data to match the expected doublet rate, and integrating the simulated doublet data with the original dataset. Each cell was then assigned a doublet score using a k-nearest neighbors (k-NN) classifier. We utilized the "doubletFinder_v3" function to label potential doublet cells (with pN set to 0.25). Based on a threshold reflecting the expected doublet rate (5%), doublets were identified and removed from the dataset.

Sample names	Raw cells	Mean reads per cell	Median genes per cell	Median UMI counts per cell	Doublet cells	Low-QC cells	Filtered cells	Mean nFeature	Mean nCount
Control-D40	5782	57,775	4,864	13,576	289	101	5392	4788	14069
Control-D90	9754	35,252	3,542	7,728	488	182	9084	3498	8277
Control-D150	7890	45,903	3,628	8,400	394	379	7117	3433	9171
Control-D200	10413	32,787	3,030	5,951	520	650	9243	2962	6661
RPGR-D40	10384	40,554	4,050	10,077	519	113	9752	4016	10564
RPGR-D90	8545	37,000	2,978	5,747	427	441	7677	2929	6632
RPGR-D150	6500	51,943	4,088	9,835	325	184	5991	4156	11473
RPGR-D200	11828	27,295	2,613	4,768	591	392	10845	2806	6389

Table 2. Quality control of scRNA-seq data based on cells.

Integration, Dimensionality reduction and Clustering. Batch effects between samples were corrected using the Harmony algorithm (v1.2.0) to ensure that comparisons were not influenced by technical variability. Once integrated, dimensionality reduction and clustering were performed to summarize expression patterns and cluster cells. The top 2,500 variable genes were identified using the "FindVariableFeatures" function of the Seurat package. PCA was performed on these genes, and the first 12 principal components were used for clustering cells with the "FindClusters" function, using a resolution parameter of 0.15. To visualize cellular clusters in two dimensions, Unified Manifold Approximation and Projection (UMAP) was employed.

Cell-type annotation. Differentially expressed genes (DEGs) were identified to understand functional differences between clusters. The "FindMarkers" function of Seurat, employing the Wilcoxon likelihood-ratio test with default parameters, was used for DEG identification. Cell type annotation was then performed to categorize cell populations. Canonical marker genes identified among the DEGs were integrated and supported by relevant literature[17,21,22].

Data Records

All the original data have been deposited to the NCBI Sequence Read Archive (SRA), with the number of SRP535874[23].

Technical validation

We considered four distinct developmental stages to interpret the transcriptome characteristics of the hiPSC-derived retinal organoids from control and RPGR group (Fig. 1a). The four stages were respectively early stage (D40)–encompassing a period of neural retina progenitor cells (NRPC) proliferation and production of a RGC layer, middle stage (D90, D150)–representing an intermediate developmental phase highlighted by differentiation of photoreceptors (PRs) and retinal interneuron population and developed stage (D200) – displaying the presence of mature outer nuclear and plexiform layers with metabolically active PRs, similar to human retina[17,24,25]. A thin outer nuclear layer (ONL), abnormal morphology of photoreceptors, and dislocation of opsins are the primary pathological features observed in patients with retinitis pigmentosa caused by RPGR mutations. Similar to the neural retina in *vivo*, RPGR-mutant ROs had significantly thinner ONL and L/M opsin mislocalization at D200 compared with the control ($P < 0.05$, Fig. 2), which is consistent with reports from other literature regarding RPGR[26–28]. Although RPGR-mutant ROs showed a higher number of L/M opsin+ and NRL+ cells, L/M opsin+ and NRL+ cells in ONL (functionally normal photoreceptor cells) were decreased in the patient group compared to the control group (Fig. 2).

After the sequencing, the raw data underwent standard processing and the Seurat package was used to carry out the downstream analysis (Fig. 1b). A comprehensive evaluation of the raw sequencing data quality is presented in Table 1. The control and RPGR groups exhibited substantial total read counts per sample, each exceeding 316 million reads. Valid barcode efficiency ranged from 91.50% to 98.40%, while sequencing saturation levels were recorded between 51.80% and 60.80%. The high quality of sequencing was evidenced by Q30 base percentages for barcodes, RNA reads, and UMI consistently exceeding 91%. Additionally, confident mapping rates to the genome and transcriptome were robust, typically above 93%, ensuring precise alignment of the reads.

Table 2 details the quality control metrics at the cell level. A total of 71,096 cells were examined, including 33,839 cells from the control group and 37,257 cells from the RPGR group. Median gene counts per cell varied from 2,613 to 4,864, and median UMI counts per cell ranged from 4,768 to 13,576. Doublet and low-quality cells were identified and excluded to maintain data integrity (Fig. 3a). After filtration, the number of cells retained per sample remained high, ensuring the reliability of the dataset. The mean nFeature and mean nCount per cell further validated the quality of the captured data (Fig. 3b), providing a solid foundation for further analysis.

Cell clustering was performed to further verify the sequencing data quality, using UMAP projecting samples into a two-dimensional plane. We observed that, the cellular distribution was generally consistent between the two groups across different developmental stages (Fig. 3c,d, e).

By analyzing the overall cellular composition of organoids at various stages, the major cell clusters differed apparently as ROs developed (Fig. 3d), and the stemness and proliferation signatures (SOX2, VSX2, PCNA) of retinal progenitor cells remarkably decreased as time progressed, consistent with the consensus that stem cells differentiate into various cell types and their renewal ability deteriorates during development and aging.

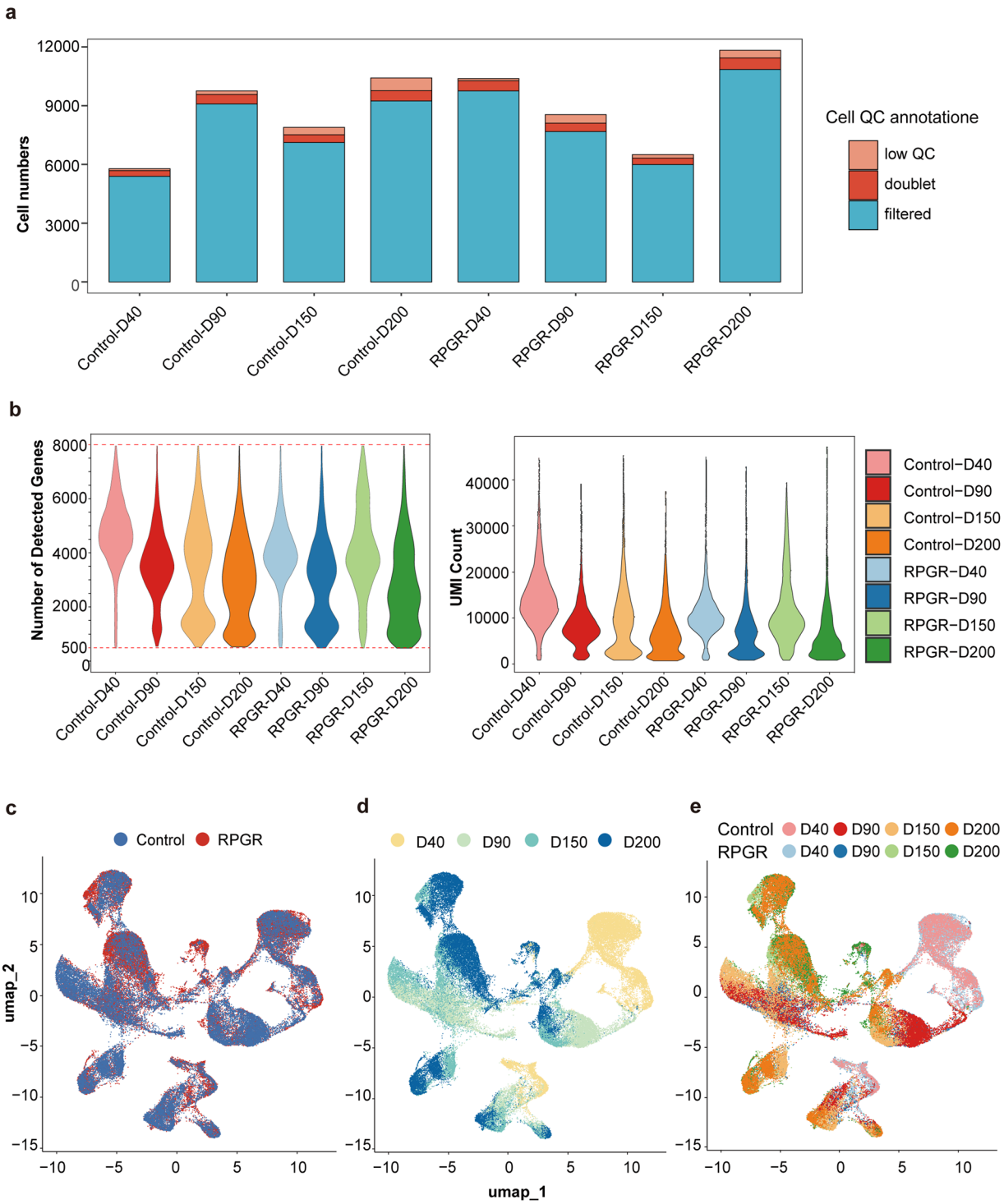

Fig. 3 Quality metrics for single-cell transcriptomics of control and RPGR-mutant retinal organoids. (**a**) Barplot displaying the numbers of doublet and low-QC cells and the number of cells retained per sample remained after filtration. (**b**) The violin plots depicting the distribution of nCount_RNA, the total number of unique molecular identifiers (UMIs) detected per cell, and nFeature_RNA, the number of unique genes or features detected per cell, across various time point. (**c**) Cell clustering UMAP displaying the distribution across the Control and RPGR groups. (**d**) UMAP illustrating the distribution across different stages. (**e**) UMAP displaying the distribution per sample.

Using cell markers identified from previous studies, we identified ten major cell types in our retinal organoid samples (Fig. 4a): early RPC (FOXP1, SFRP2), late RPC (RLBP1, CRYM), RGC (SNCG, EBF1), BC (NETO1, GRIK1, TMEM215, VSX1), HC (ONECUT1, TFAP2B), AC (GAD1, TFAP2A), photoreceptor (PR) precursor (OTX2, PRDM1), cone (ARR3, GUCA1C, GNAT2), rod (NRL, GNAT1, GNGT1) and müller cell (AQP4, GFAP,

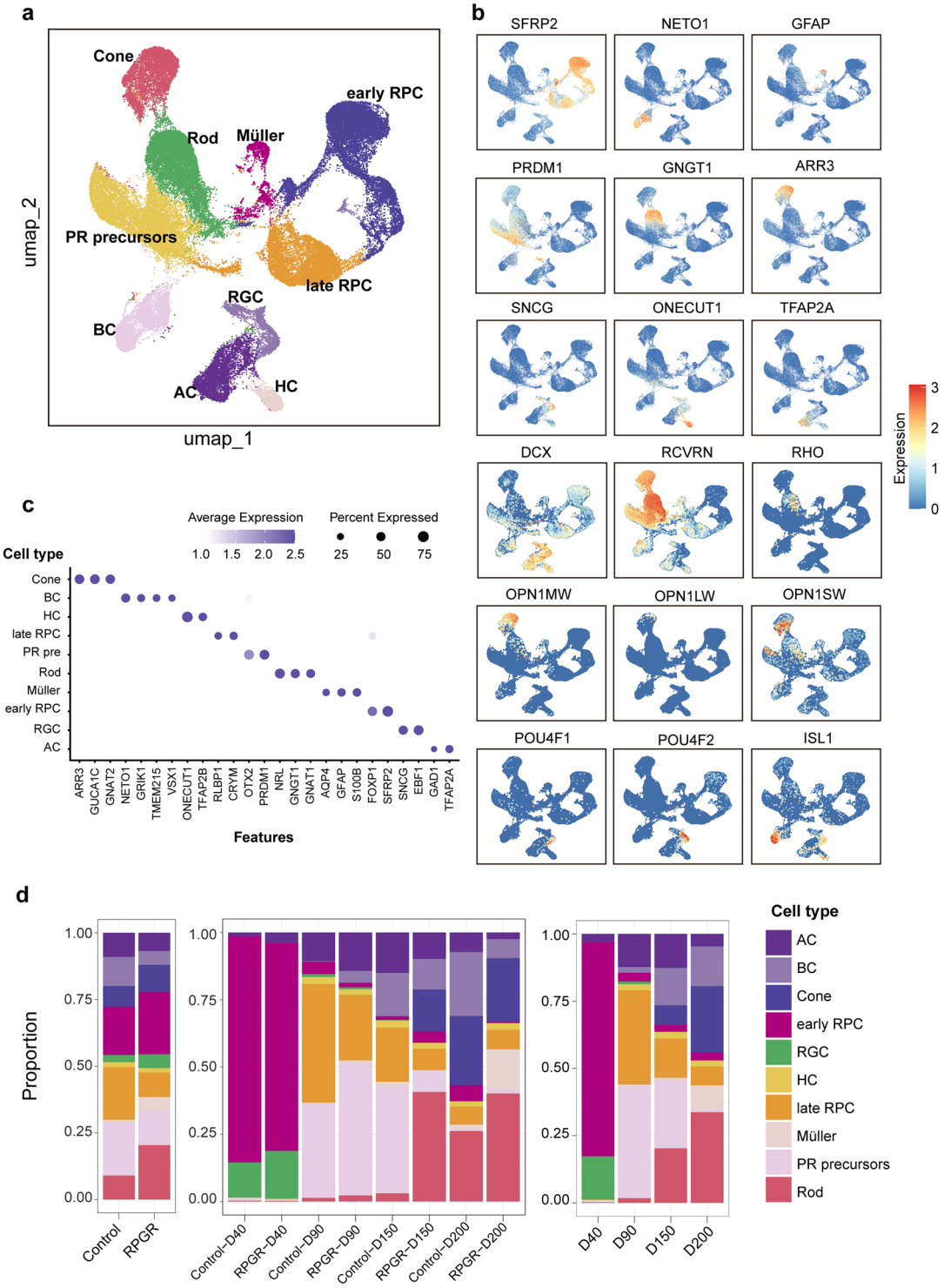

Fig. 4 Clustering and annotation of the control and RPGR-mutant retinal organoids sc-RNAseq data. (**a**) UMAP presentation of 10 clusters with different colors representing various cell types of ROs. (**b**) UMAP visualization of cell type-specific gene activity scores. (**c**) Dotplot displaying marker genes of the 10 various cell types identified from the scRNAseq data. (**d**) Comparison between stack diagram showing the cell type proportions across different group, across different developing stages, and across each RO sample from the control and RPGR groups and four stages.

S100B)[17,21,22]. Cell-type-specific gene expression patterns across 10 distinct cell types were further delineated (Fig. 4b). For example, cones exhibited distinct peaks of expression for ARR3, GUCA1C, and GNAT2, whereas rods showed notable expression of NRL, GNAT1 and GNGT1. Similarly, the dot plot showed the marker genes specifically enriched in certain cells but not observed in other cell types (Fig. 4c) and the heatmap analysis

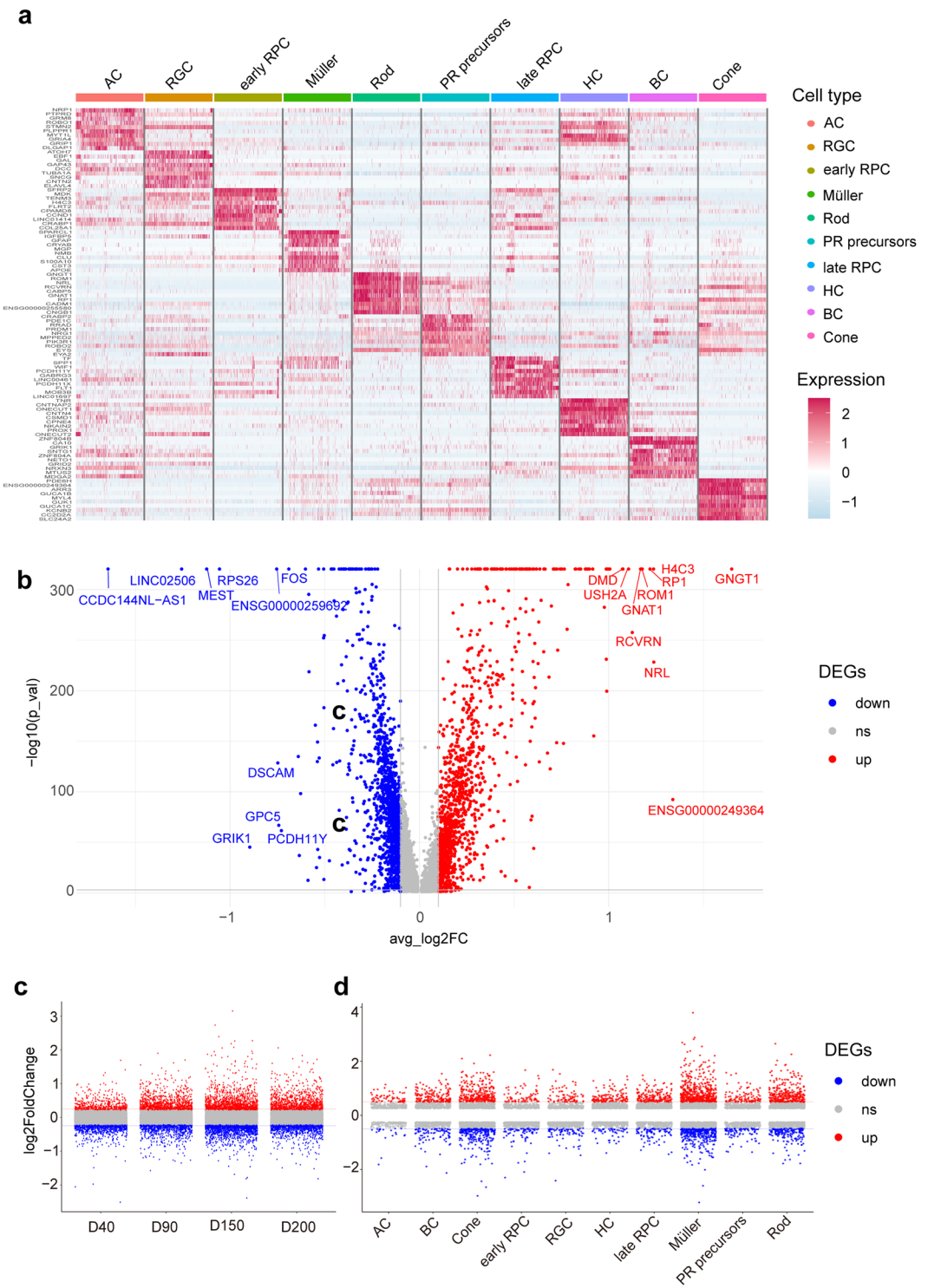

Fig. 5 Differentially expressed genes (DEGs) between the control and RPGR group. (**a**) The heatmap showing the expression patterns of selected genes across different retinal cell types. (**b**) The volcano plot of DEGs between control and RPGR-mutant ROs. (**c**) The volcano plot of DEGs between control and RPGR-mutant ROs across four developmental time points. (**d**) The volcano plot of DEGs identified for each cell type between control and RPGR-mutant ROs.

revealed a more detailed description of the gene expression patterns within these cell clusters (Fig. 5a), highlighting the superior quality of our sequencing data and its consistency with the molecular characteristics of the cells. More details of the differences in cell type composition between control and RPGR-mutant ROs spanning different developmental days derived from single-cell sequencing data were shown in Fig. 4d, providing insights into the cellular heterogeneity and developmental trajectories influenced by the RPGR mutation. Meanwhile,

the comparative analysis of gene expression between control and RPGR-mutant ROs at sequential time points and across various cell types was presented (Fig. 5b–d and table S1, S2, S3). Notably, an increase in cone- and rod-related gene expression was observed in RPGR-mutant ROs during the late developmental stage compared to controls, aligning with the observed increase in L/M opsin + and NRL + cells in immunofluorescence images. These results are different from those observed in RPGR animal models. However, similar findings have been discovered in retinal organoid disease models with other gene mutations. Nathaniel K. Mullin *et al.* found that rod-committed photoreceptor cells form and persist throughout life in NR2E3-mutant ROs, naming these rods 'divergent rods.' These NR2E3-null rods additionally misexpress several cone-specific phototransduction genes[29]. Another transcriptomic analysis of RP2-knockout (KO) ROs revealed that the percentage of cone arrestin-positive cells was significantly increased in the RP2-KO ROs compared to controls[30]. Together, our data provide a roadmap for the development of human photoreceptor cells, indicating that the observed upregulation and downregulation of specific genes in the retina reflect crucial functional changes, which become increasingly pronounced as differentiation advances.

In summary, these analyses underscore the dataset's high quality and reveal potential changes under RPGR mutant conditions. This dataset could offer powerful tools and clear direction for advanced studies investigating the molecular mechanisms underlying RPGR mutation effects on retinal organoid development and identifying potential therapeutic targets.

Usage Notes

The scRNA-seq data processing pipeline was run on the Linux operating system. All R source code used for downstream data analyses and visualization are provided online (https://figshare.com/articles/journal_contribution/Code/26240633, where https://doi.org/10.6084/m9.figshare.26240633 is the DOI)[31].

Code availability

The codes used to analyze the data in this study were available online (https://figshare.com/articles/journal_contribution/Code/26240633)[31].

Received: 23 July 2024; Accepted: 12 November 2024;
Published online: 26 November 2024

References

1. De Silva, S. R. *et al.* The X-linked retinopathies: Physiological insights, pathogenic mechanisms, phenotypic features and novel therapies. *Prog. Retin. Eye Res.* **82**, 100898 (2021).
2. Kamde, S. P. & Anjankar, A. Retinitis Pigmentosa: Pathogenesis, Diagnostic Findings, and Treatment. *Cureus* **15**, e48006 (2023).
3. Vinikoor-Imler, L. C., Simpson, C., Narayanan, D., Abbasi, S. & Lally, C. Prevalence of RPGR-mutated X-linked retinitis pigmentosa among males. *Ophthalmic Genet.* **43**, 581–588 (2022).
4. Chiang, J. P. W. *et al.* Development of High-Throughput Clinical Testing of RPGR ORF15 Using a Large Inherited Retinal Dystrophy Cohort. *Invest. Ophthalmol. Vis. Sci.* **59**, 4434–4440 (2018).
5. Georgiou, M. *et al.* Extending the phenotypic spectrum of PRPF8, PRPH2, RP1 and RPGR, and the genotypic spectrum of early-onset severe retinal dystrophy. *Orphanet J. Rare Dis.* **16**, 128 (2021).
6. Hong, D. H., Yue, G., Adamian, M. & Li, T. Retinitis pigmentosa GTPase regulator (RPGRr)-interacting protein is stably associated with the photoreceptor ciliary axoneme and anchors RPGR to the connecting cilium. *J. Biol. Chem.* **276**, 12091–12099 (2001).
7. Megaw, R. *et al.* Gelsolin dysfunction causes photoreceptor loss in induced pluripotent cell and animal retinitis pigmentosa models. *Nat. Commun.* **8**, 271 (2017).
8. Hong, D. H. *et al.* A retinitis pigmentosa GTPase regulator (RPGR)-deficient mouse model for X-linked retinitis pigmentosa (RP3). *Proc. Natl. Acad. Sci. USA* **97**, 3649–3654 (2000).
9. Rao, K. N. *et al.* Loss of human disease protein retinitis pigmentosa GTPase regulator (RPGR) differentially affects rod or cone-enriched retina. *Hum. Mol. Genet.* **25**, 1345–1356 (2016).
10. Khanna, H. More Than Meets the Eye: Current Understanding of RPGR Function. *Adv. Exp. Med. Biol.* **1074**, 521–538 (2018).
11. Awadh Hashem, S., Georgiou, M., Ali, R. R. & Michaelides, M. RPGR-Related Retinopathy: Clinical Features, Molecular Genetics, and Gene Replacement Therapy. *Cold Spring Harb. Perspect. Med.* a041280 https://doi.org/10.1101/cshperspect.a041280 (2023).
12. Lancaster, M. A. & Knoblich, J. A. Organogenesis in a dish: modeling development and disease using organoid technologies. *Science* **345**, 1247125 (2014).
13. Llonch, S., Carido, M. & Ader, M. Organoid technology for retinal repair. *Dev. Biol.* **433**, 132–143 (2018).
14. Clark, B. S. *et al.* Single-Cell RNA-Seq Analysis of Retinal Development Identifies NFI Factors as Regulating Mitotic Exit and Late-Born Cell Specification. *Neuron* **102**, 1111–1126.e5 (2019).
15. Sridhar, A. *et al.* Single-Cell Transcriptomic Comparison of Human Fetal Retina, hPSC-Derived Retinal Organoids, and Long-Term Retinal Cultures. *Cell Rep.* **30**, 1644–1659.e4 (2020).
16. Collin, J. *et al.* Deconstructing Retinal Organoids: Single Cell RNA-Seq Reveals the Cellular Components of Human Pluripotent Stem Cell-Derived Retina. *Stem Cells* **37**, 593–598 (2019).
17. Cowan, C. S. *et al.* Cell Types of the Human Retina and Its Organoids at Single-Cell Resolution. *Cell* **182**, 1623–1640.e34 (2020).
18. Loh, Y.-H. *et al.* Generation of induced pluripotent stem cells from human blood. *Blood* **113**, 5476–5479 (2009).
19. Okita, K. *et al.* An Efficient Nonviral Method to Generate Integration-Free Human-Induced Pluripotent Stem Cells from Cord Blood and Peripheral Blood Cells. *Stem Cells* **31**, 458–466 (2013).
20. Capowski, E. E. *et al.* Reproducibility and staging of 3D human retinal organoids across multiple pluripotent stem cell lines. *Dev. Camb. Engl.* **146**, dev171686 (2019).
21. Lyu, Y. *et al.* Implication of specific retinal cell-type involvement and gene expression changes in AMD progression using integrative analysis of single-cell and bulk RNA-seq profiling. *Sci. Rep.* **11**, 15612 (2021).
22. Gautam, P. *et al.* Multi-species single-cell transcriptomic analysis of ocular compartment regulons. *Nat. Commun.* **12**, 5675 (2021).
23. *NCBI Sequence Read Archive* https://identifiers.org/ncbi/insdc.sra:SRP535874 (2024).
24. Wahle, P. *et al.* Multimodal spatiotemporal phenotyping of human retinal organoid development. *Nat. Biotechnol.* https://doi.org/10.1038/s41587-023-01747-2 (2023).
25. Browne, A. W. *et al.* Structural and Functional Characterization of Human Stem-Cell-Derived Retinal Organoids by Live Imaging. *Invest. Ophthalmol. Vis. Sci.* **58**, 3311–3318 (2017).

26. Sladen, P. E. *et al*. AAV-RPGR Gene Therapy Rescues Opsin Mislocalisation in a Human Retinal Organoid Model of RPGR-Associated X-Linked Retinitis Pigmentosa. *Int. J. Mol. Sci.* **25**, 1839 (2024).
27. Deng, W.-L. *et al*. Gene Correction Reverses Ciliopathy and Photoreceptor Loss in iPSC-Derived Retinal Organoids from Retinitis Pigmentosa Patients. *Stem Cell Rep.* **10**, 1267–1281 (2018).
28. Chahine Karam, F. *et al*. Human iPSC-Derived Retinal Organoids and Retinal Pigment Epithelium for Novel Intronic RPGR Variant Assessment for Therapy Suitability. *J. Pers. Med.* **12**, 502 (2022).
29. Mullin, N. K. *et al*. NR2E3 loss disrupts photoreceptor cell maturation and fate in human organoid models of retinal development. *J. Clin. Invest.* **134**, e173892 (2024).
30. Lane, A. *et al*. Modeling and Rescue of RP2 Retinitis Pigmentosa Using iPSC-Derived Retinal Organoids. *Stem Cell Rep.* **15**, 67–79 (2020).
31. Li, T. *et al*. Single-Cell Transcriptomic Dataset of RPGR Retinitis Pigmentosa Patient-Derived Retinal Organoids https://doi.org/10.6084/m9.figshare.26240633.v5 (2024).

Acknowledgements

This work was supported by the National Key Research and Development Program of China (Grant Numbers 2020YFA0112700, 2020YFA0112703), the National Natural Science Foundation (Grant Numbers 82271085 and 82171055) of the People's Republic of China, Shanghai Municipal Commission of Science and Technology (Grant Numbers 21S11905900, 24J12800200), Xuhui Hospital and Regional Cooperation Project (Grant Number 23XHYD-28).

Author contributions

Ting Li wrote the manuscript and contributed to the culture of ROs; Yuting Ma, Yingke Zhao and Zhixu Qiu performed the bioinformatics processing of the scRNA-seq data. Yun Cheng, Hongli Liu, Daowei Zhang, Jiawen Wu and Junfeng Li contributed to the ROs culture and prepared them for single-cell analysis. Shenghai Zhang and Jihong Wu conceptualized the experiment, approved and authored the final manuscript. All authors approved the final version of the manuscript.

Competing interests

The authors declare no competing interests.

Additional information

Supplementary information The online version contains supplementary material available at https://doi.org/10.1038/s41597-024-04124-z.

Correspondence and requests for materials should be addressed to S.Z. or J.W.